REAL TIME OPTICAL DIAGNOSTICS IN LASER ETCHING AND DEPOSITION

IRVING P. HERMAN, HUA TANG, and PATRICK P. LEONG
Department of Applied Physics and the Microelectronics Sciences Laboratories,
Columbia University, New York, NY 10027.

ABSTRACT

Optical probing of laser-assisted chemical reactions on surfaces in real time can help explain and control these processes. Raman microprobe spectroscopy and micro laser induced fluorescence are the two optical probes employed here to investigate several examples of localized laser surface reactions. Raman microprobe analysis is used to monitor in real time the CuCl and $CuCl_2$ products on the surface during local laser etching of copper films by Cl_2 and the concomitant loss of the Cu_2O passivation layer. It is also used to follow the production of Cu_2O during the laser oxidation of Cu. Polarization Raman analysis is utilized to identify and analyze partially molten silicon during laser heating in vacuum and during the etching of silicon by chlorine. Laser induced fluorescence is used as a real time microprobe of desorbed products during local laser-assisted etching of Si and Al surfaces.

INTRODUCTION

Optical spectroscopic methods have long been used as nondestructive, in situ probes of the gas phase and of the film itself during thin film processing. Film properties, such as composition, crystallinity, and stress, and the film temperature can be measured with optical probes, which can also be utilized to determine the identity, concentration, and energy level distribution of reactants and products in the gas medium above the films. The focus of this work is on the use of optical diagnostics to probe laser microchemical reactions on surfaces in real time. Optical probes with very high spatial resolution are needed in such studies because the lateral spatial extent of the surface modification is typically ~ 1 μm.

The most common and the simplest optical probes of films in laser-assisted processing are transmission and reflection spectroscopy.[1,2] By examining film absorption and interference effects, the film thickness can be probed in real time. The emphasis of this work is on the use of another technique, Raman microprobe spectroscopy, to probe films during and in situ after laser processing. Raman spectroscopy has several strengths, particularly the unique information it can provide about semiconductor and insulator films and its insensitivity to surface roughness, that often outweigh its principal

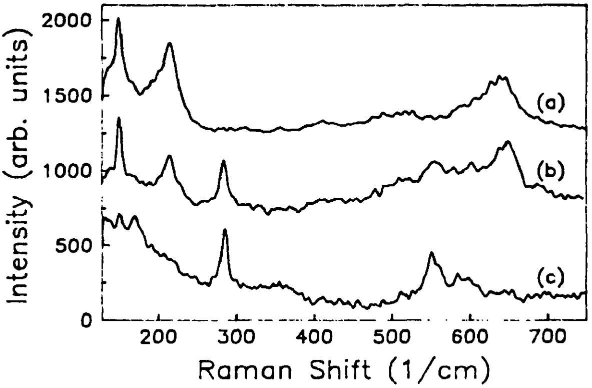

Figure 1. The Raman spectrum (a) before, (b) during, and (c) after laser etching of a 1.4 μm-thick copper film on glass (4880 Å, 60 mW, 10 Torr Cl_2 during etching). (Adapted from Ref. 3.)

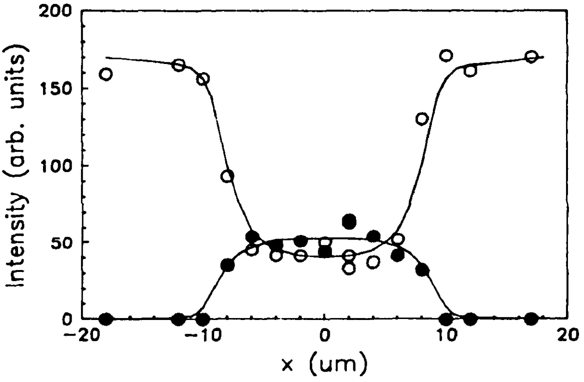

Figure 2. Raman scattering intensity of CuCl (~ 125 cm^{-1} feature, open circles) and $CuCl_2$ (282 cm^{-1} peak, filled circles) in a transverse scan across a laser-etched line in a CuCl film-atop-Cu film on a glass substrate (4880 Å, 80 mW, 13 Torr Cl_2, 5 μm/sec scan speed). This microprobe scan shows the varying amounts of CuCl and $CuCl_2$.

disadvantage, namely, the weak intensity of spontaneous Raman scattering signals. This paper will demonstrate how Raman microprobe scattering can be used to determine the composition, temperature, phase and doping of regions near the surface during direct laser writing. The use of laser induced fluorescence to probe products desorbed during localized laser etching will also be discussed.

In the experiments presented here, a visible line from an argon-ion laser is typically focused to a 0.8 μm spot size (halfwidth at 1/e intensity) and scanned along the surface in the presence of a reactive gas. This laser heats the surface locally, inducing a pyrolytic reaction. When this same focused laser is also used for the Raman microprobe, this diagnostic analyzes the moving reaction front with a lateral resolution of ~ 2 μm and a depth resolution that is one half the optical absorption depth of the film. Parallel detection of the dispersed collected light, here with an intensified diode array, enables rapid collection of Raman spectra. Measurements can be made in real time during processing and also in situ after processing with this experimental configuration.

RAMAN ANALYSIS OF COMPOSITION CHANGES

The limiting step in both laser and conventional dry etching of metals with halogens is often the desorption of the metal halide etch product. Raman analysis can be used to probe these residual metal halides during scanned laser pyrolytic etching of copper films on glass by a chlorine reactant, as is illustrated in Figure 1.[3] The Raman spectrum of the film before etching (Figure 1a) shows three peaks due to the Cu_2O passivation layer that was previously grown on the surface. Figure 1b is a Raman spectrum taken in real time during the laser etch, with the peak near 282 cm^{-1} showing the growth of $CuCl_2$. After etching, another spectrum was taken in situ along the laser etch line (Figure 1c). $CuCl_2$ and CuCl, diagnosed by the broad peak near 125 cm^{-1}, are seen while very little Cu_2O remains. Figure 2 shows the Raman peak height of the 282 cm^{-1} feature of $CuCl_2$ and the ~ 125 cm^{-1} feature of CuCl at various positions laterally across a scanned line that was etched on a CuCl film/Cu film on a glass substrate. This shows that the ratio $CuCl_2$/CuCl is maximum at the center, which is where the temperature is highest during laser heating.

Baufay et al.[1] and Andrew[2] have used reflectivity probes to investigate the early stages of oxidation of thin Cu films on glass substrates that were heated by cw argon-ion laser irradiation in air. Those experiments used two beams, where the spot size of the heating laser (~ 200 μm) was much larger than that of the probe (~ 20 μm). By following the fringes in the intensity of the reflected beam, they showed that the rate of growth of Cu_2O depended on the net power absorbed by the film at that time. We have begun to use the Raman microprobe to examine in real time laser-assisted oxidation of copper films,

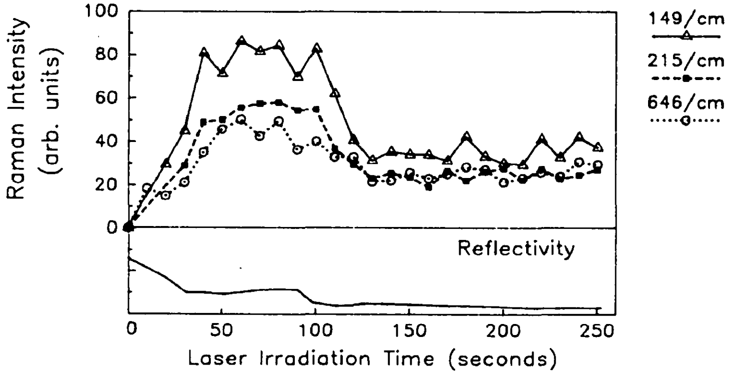

Figure 3. The strengths of the Cu_2O Raman peaks during laser oxidation of 1.4 μm-thick copper films in air vs. time (4880 Å, 30 mW, no scanning). Raman data plotted at time t were integrated from t – 10 sec to t after irradiation began. Also plotted is the reflected intensity of the heating laser.

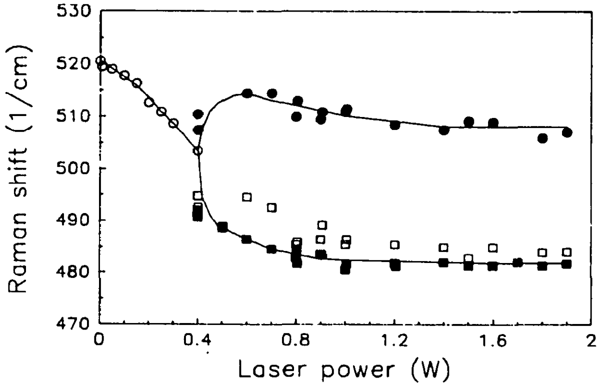

Figure 4. Raman lineshifts during laser heating of c-Si with a stationary laser vs. laser power (P < 0.4 W: z(x, y)z̄ - open circles; P > 0.4 W: z(x, y)z̄ - filled circles and open squares, and z(x, x)z̄ - filled squares).

making use of reflectivity as a second optical probe. In the preliminary experiments presented here, the same laser has been used to heat the surface and thereby to promote the oxidation of the copper film in air, to serve as a source of photons for Raman scattering, and to serve as the reflection probe (~ 2 μm spot size).

Raman analysis shows that there is a gradual appearance of a Cu_2O spectrum as the oxidation of the Cu film proceeds under laser irradiation. The spectrum has three dominant peaks at 149, 215, and 646 cm^{-1}, and looks like the spectrum of copper oxide obtained by oxidation of a copper film in air by conventional heating methods, as shown in Figure 1a. Only the 215 cm^{-1} peak, the two-phonon mode $2\Gamma_{12^-}$, is allowed in the Raman scattering of Cu_2O crystals. As demonstrated in [4], the other two peaks appear after the copper oxide is made amorphous by ion implantation. Consequently, laser oxidized Cu appears to be amorphous.

Figure 3 shows the growth of the three main Raman features vs. time, along with the time dependence of the reflected intensity of the incident laser, for $P = 30$ mW. The intensity of each Raman peak increases monotonically with time and the reflected power decreases, until ~ 40 sec after the start of irradiation. Then the Raman signals remain constant until ~ 100 sec, after which they decrease to lower values. A marked change in the reflection spectrum also occurs at about this time. These observations suggest that the Cu_2O film is growing monotonically with time until 40 sec, and then the film remains unchanged for another 60 sec. There is still some Cu_2O in the film for times after 100 sec, but the change occurring at 100 sec has not yet been identified. Qualitatively similar behavior occurs for different laser powers, with the time scales decreasing with increasing power. Interference effects in the reflected and Raman scattered beams are not expected in these one-beam experiments because the probe analyzes a localized copper oxide layer whose thickness probably varies across the probe laser. Interference effects are expected in planned two-beam experiments.

RAMAN ANALYSIS OF TEMPERATURE AND PHASE CHANGES

Changes in the Raman lineshift and linewidth, and in the polarization properties of the scattered light can be used to probe localized temperature and phase changes in semiconductors. In Raman analysis of Si (001), in backscattered configuration using a low intensity probe, the LO phonon peak appears with $z(x, y)\bar{z}$ polarization orientation, but not with $z(x, x)\bar{z}$ orientation. When the same stationary laser is used to heat and probe the Si wafer in vacuum, this LO phonon peak is still seen only with $z(x, y)\bar{z}$ orientation and the Raman shift decreases from 520 to 502 cm^{-1} as the power P of the laser is increased to 400 mW (Figure 4), which is the threshold for melting P_m (for a 0.8 μm spot size). This shift

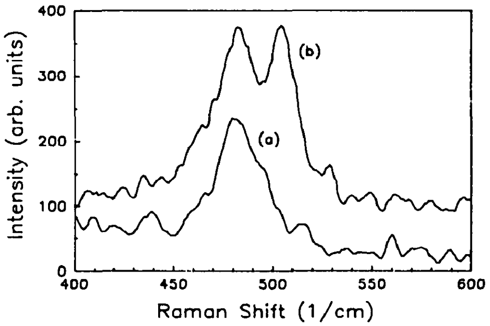

Figure 5. Raman spectra of a Si substrate that was partially molten due to laser heating, taken in the (a) z(x, x)z̄ and (b) z(x, y)z̄ polarization orientations (5145 Å, 1.2 W, averaged for the first 0.5 sec). (From Ref. 5.)

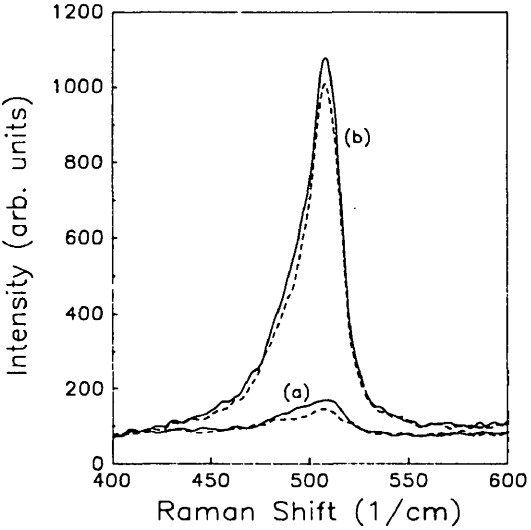

Figure 6. Real-time Raman spectra of laser melting (120 Torr Ar, unbroken lines) and laser etching (0.5 Torr Cl_2/120 Torr Ar, dashed lines) of Si (001) in the (a) z(x, x)z̄ and (b) z(x, y)z̄ polarization orientations (5145 Å, 1.6 W, 150 µm/sec scan speed).

measured in this microheating experiment at melting, 502 cm^{-1}, is much larger than the optical phonon frequency at the melting point, 482 cm^{-1},[5] because the microprobe averages laterally for a distance of ~ 2 μm over the nonuniform temperature profile.[6]

The appearance of a peak in the $z(x, x)\bar{z}$ orientation can indicate either that the substrate surface is no longer (001), as can occur because of localized etching, or that the [100] and [010] directions on the surface have rotated, which can occur in partially molten silicon where solid regions are floating in the melt or in solid silicon when there is grain reorientation or polycrystallinity after solidification. For laser powers $P > P_m$, there are solid regions at the melting point temperature floating in the melt. This is indicated by the single peak with $z(x, x)\bar{z}$ orientation and the lower energy peak with $z(x, y)\bar{z}$ orientation near 482 cm^{-1} in Figure 5. These spectra were taken with a stationary, nonscanning laser. Because these solid silicon regions are in the molten bath, their temperature is pegged at the melting temperature, 1690 K, and the Raman signal is fixed at the phonon frequency of solid silicon at the melting point. Molten silicon has no Raman spectrum. The higher energy peak seen with $z(x, y)\bar{z}$ polarization corresponds to heated solid Si (001) surrounding the partially molten zone.

These observations can be used to help characterize localized deposition and etching of silicon even when the laser is scanned across the surface. For instance, in a previous study Raman scattering was used to probe laser pyrolytic deposition of Si by local CVD in real time.[7] The unpolarized Raman spectra taken in that study typically had a large peak near 480 cm^{-1} and a weaker peak or shoulder near 510 cm^{-1}. This resembles the $z(x, y)\bar{z}$ spectrum in Figure 5, and suggests that the silicon deposited in that study was initially partially molten.

We are currently using polarized Raman scattering to study the etching of Si (001) during local laser heating in the presence of chlorine. Treyz and coworkers[8] have demonstrated that this etching process occurs very quickly only when the silicon at the surface is molten, and that the etch rate increases as the fraction of molten material in partially molten regions increases. Addition of argon as a buffer gas was shown to slow the reaction. They developed a model that predicts that the rate of silicon etching depends on the fraction of silicon that is molten at the laser front.

Figure 6 shows the polarized Raman spectra at the scanning laser front for neat 120 Torr Ar and for a 0.5 Torr Cl_2/120 Torr Ar mixture. The laser power 1.6 W far exceeds that needed for melting. Because the laser is scanning along the surfac at 150 μm/sec in these etching experiments, the conditions are somewhat different than those for the static beam experiments depicted in Figures 4 and 5. The etching experiment was designed to have an etch rate slow enough to avoid geometric complications in Raman scattering

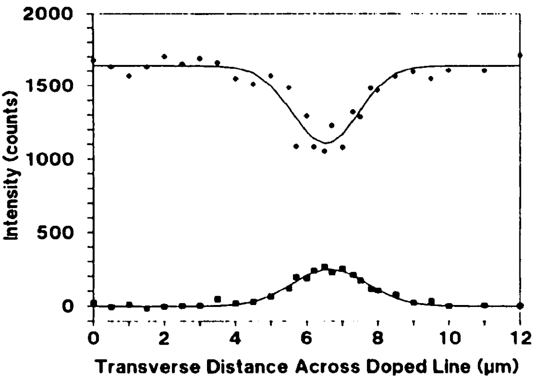

Figure 7. Raman intensities of LO and TO phonon peaks (upper and lower curves, respectively) measured across a line in GaAs which was doped by Zn using direct laser writing. (From Ref. 10.)

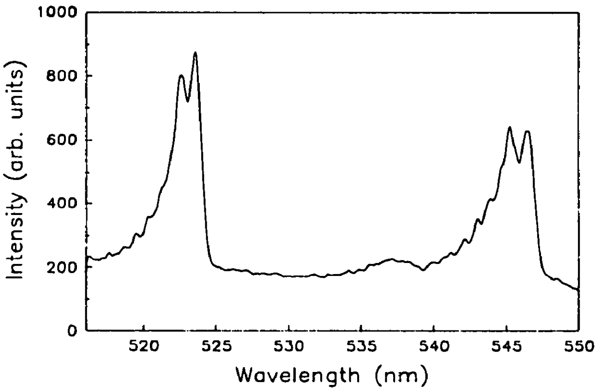

Figure 8. MicroLIF spectra of HSiCl taken during laser etching of Si by HCl (4880 Å, 860 mW, 100 Torr HCl + 330 Torr Ar, 30 µm/sec scan speed).

associated with deep etch trenches. During the scans with pure argon the silicon is molten at the laser front. Though there is no etching during these scans, there can still be a flow of liquid silicon away from the center because of surface tension. The $z(x, y)\bar{z}$ spectra during scans with either gas mixture are essentially identical, and are dominated by one asymmetric feature that peaks near 510 cm^{-1}. This feature looks very much like the high energy peak in the static scan in Figure 5, and it represents very hot, solid Si (001).

The $z(x, x)\bar{z}$ feature is much smaller for both gas conditions. With pure argon the spectrum peaks near 510 cm^{-1}, as does the $z(x, y)\bar{z}$ feature, which suggests that it is very hot solid silicon with a nonuniform temperature profile that is oriented differently than the initial substrate (as described above). However, this feature has a very long tail towards lower energies and is much broader than the $z(x, y)\bar{z}$ peak. The $z(x, x)\bar{z}$ signal is significantly smaller with the chlorine/argon mixture than with argon, and has a peak near 510 cm^{-1} and possibly a shoulder near 484 cm^{-1}. This latter feature is probably due to solid silicon pegged at the melting temperature in a molten bath, and is probably in the other three spectra also but is hidden by the larger 510 cm^{-1} feature. Because of etching, there is less reoriented silicon and possibly less partially molten silicon in steady state than with Ar.

RAMAN ANALYSIS OF LOCAL CHANGES IN DOPING

Doping can modify the Raman spectrum of a semiconductor in three ways: (1) single particle or collective modes of free carriers can alter the phonon peaks of the undoped sample, (2) lattice disorder caused by the dopant atoms can "soften" the Raman selection rules of the undoped sample, and (3) new modes due to local vibrations of the dopant can appear.[9] This second contribution has been used to monitor the localized laser doping of Zn in GaAs.[10] As is shown in Figure 7, both the LO and TO phonon modes of GaAs (near 292 and 268 cm^{-1}) appear in the Raman spectrum in doped regions, while only the LO mode appears in undoped regions. The laser doped line is measured to be 2.0 μm wide by scanning the probe laser across this feature. Though this measurement was made ex situ, it could easily be implemented in situ and be used as a real time probe of laser doping.

MICRO LASER INDUCED FLUORESCENCE

Laser induced fluorescence (LIF) can be used to measure the concentration of many desorbed reaction products, particularly diatomics and some triatomics, during etching and deposition reactions. It is well suited to the study of localized laser reactions when tightly focused lasers are used to spatially resolve the gas-phase products. In the simplest arrangement, one laser can be focused onto the surface to induce the reaction locally and to

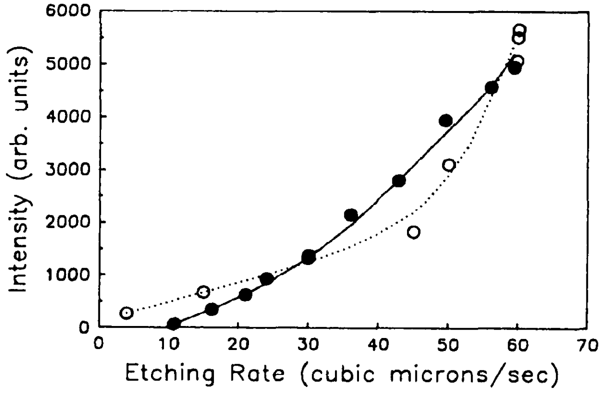

Figure 9. Signal strength of microLIF spectra of HSiCl taken during laser etching of Si by HCl vs. the volume etching rate (4880 Å, 860 mW; open circles: 100 Torr Cl_2, 2 - 50 µm/sec scan speed; filled circles: 30 µm/sec scan speed and 0 - 200 Torr Cl_2).

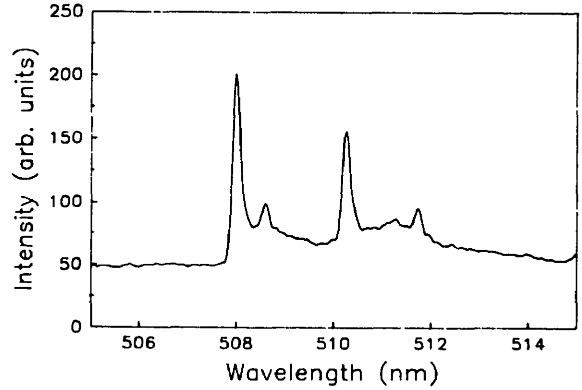

Figure 10. MicroLIF of AlO desorbed from aluminum oxide layer on an Al film (4880 Å, 2.2 W, 58 Torr Ar, 20 µm/sec scan speed).

serve simultaneously as a source of photons for micron-dimension LIF (microLIF) in the focal region above the surface. Even with a laser spot size of ~ 2 μm on the surface, the spatial resolution is only ~ 100 μm^3 because all products in the laser focal region above the surface are detected. Though this resolution can be improved, the current method at least provides a simple method for identification of desorbed products.

Etching of Si (100) by local laser heating of the substrate in the presence of HCl was studied by using 4880 Å to heat the silicon and to excite the $A(^1A'')$ or $a(^3A'')$ (010) ← $X(^1A')$ (010) transition in the HSiCl etch product. LIF of this radical from A → X has been seen during Si CVD using a SiH_2Cl_2 reactant[11] and during local laser CVD of Si from $SiCl_4/H_2$ mixtures and local laser etching of Si by HCl.[12] Figure 8 shows the $A(^1A'')$ or $a(^3A'')$ (000) → $X(^1A')$ (020) and (030) fluorescence from HSiCl [near 523 and 547 nm, respectively] that is observed in the ~ 100 μm^3 volume above the moving etching front.

In Figure 9, the intensity of the microLIF signal is plotted vs. the volume etching rate. The etching rate was determined by multiplying the laser scan rate by the etch cross-section measured <u>ex situ</u> by profilometry. Two runs were conducted, both with the same laser power 860 mW and same laser focus 2 μm. In one case the scan speed was kept constant (30 μm/sec) and the HCl pressure was varied from 0 to 200 Torr, while in the other the HCl pressure was held constant (100 Torr) and the scan rate was varied from 2 to 50 μm/sec. Though there are differences in these two curves, even when plotted in this normalized manner, these data show that the LIF intensity of HSiCl increases somewhat faster than linearly with the rate of etching of Si atoms from the surface regardless of the details of the etching process. This microLIF signal may serve as a good probe of the local etch rate.

In related studies, gas-phase AlO has been detected during local laser heating of oxidized aluminum surfaces by using microLIF, as is shown in Figure 10. MicroLIF signals are seen only with $P > 2.1$ W. Temperature calculations suggest that the Al near the surface is molten in this power range (T_{melt} for Al is 933 K). The 4880 Å laser both heats the Al_2O_3/Al film system and excites the $B^2\Sigma^+$ (v' = 0, K" = 49) ← $X^2\Sigma^+$ (v' = 0, K' = 48) and the $B^2\Sigma^+$ (v' = 1, K" = 56) ← $X^2\Sigma^+$ (v' = 1, K' = 57) transitions in the AlO products.[13,14] No $B^2\Sigma^+ \rightarrow X^2\Sigma^+$ microLIF is observed with laser heating in vacuum. The microLIF intensity increases rapidly with added Ar gas until 50 Torr, remains constant to 200 Torr, and decreases slowly with increasing pressure. The added Ar may have three effects: (1) increasing the local AlO density by forcing diffusive transport, (2) collisionally relaxing AlO into states absorbing the laser, (3) and at high pressure, collisionally relaxing AlO states absorbing the laser.

CONCLUDING REMARKS

Optical spectroscopy has been applied with micrometer resolution to monitor direct laser writing processes. These optical diagnostics are also useful in studying selected-area reactions in other types of thin film processing.

ACKNOWLEDGMENTS

The authors would like to acknowledge the financial support by the Office of Naval Research and IBM, and to thank T. Licata, R. Osgood, and F. Magnotta who collaborated in some of the reported studies.

REFERENCES

1. L. Baufay, F. Houle, and R. J. Wilson, J. Appl. Phys. 61, 4640 (1987).
2. R. Andrew, Appl. Phys. B41, 205 (1986).
3. H. Tang and I. P. Herman, J. Vac. Sci. Technol. A8, 1608 (1990).
4. D. Powell, A. Compaan, J. R. Macdonald, and R. A. Forman, Phys. Rev. B12, 20 (1975).
5. H. Tang and I. P. Herman, Phys. Rev. B (in press).
6. G. D. Pazionis, H. Tang, and I. P. Herman, IEEE J. Quantum Electron. 25, 976 (1989).
7. F. Magnotta and I. P. Herman, Appl. Phys. Lett. 48, 195 (1986); I. P. Herman, F. Magnotta, and D. E. Kotecki, J. Vac. Sci. Technol. A4, 659 (1986).
8. G. V. Treyz, R. Beach, and R. M. Osgood, Jr., J. Vac. Sci. Technol. B6, 37 (1988).
9. G. Abstreiter, M. Cardona, and A. Pinczuk, in Light Scattering in Solids IV, Topics in Appl. Phys. 54, edited by M. Cardona and G. Guntherodt (Springer, New York, 1984), p. 5.
10. T.J. Licata, D.V. Podlesnik, H. Tang, I.P. Herman, R.M. Osgood, Jr., and S.A. Schwarz, J. Vac. Sci. Technol. A8, 1618 (1990).
11. P. Ho and W. G. Breiland, Appl. Phys. Lett. 43, 125 (1983).
12. F. Magnotta, Microbeam Analysis-1987, Ed. R. H. Geiss, San Francisco Press, San Francisco, CA, p. 153, and personal communication.
13. L. Pasternack and P. J. Dagdigian, J. Chem. Phys. 67, 3854 (1977).
14. H. Partridge, S. R. Langhoff, B. H. Lengsfield, III and B. Liu, J. Quant. Spectrosc. Radiat. Transfer 30, 449 (1983).